HHS Public Access

Author manuscript

Mol Imaging Biol. Author manuscript; available in PMC 2016 April 01.

Published in final edited form as:

Mol Imaging Biol. 2015 April ; 17(2): 284–294. doi:10.1007/s11307-014-0783-7.

Patient-Specific Dosimetry Using Pretherapy [^{124}I]m-iodobenzylguanidine ([^{124}I]mIBG) Dynamic PET/CT Imaging Before [^{131}I]mIBG Targeted Radionuclide Therapy for Neuroblastoma

Shih-ying Huang[1], **Wesley E. Bolch**[2], **Choonsik Lee**[3], **Henry F. Van Brocklin**[1], **Miguel H. Pampaloni**[1], **Randall A. Hawkins**[1], **Aimee Sznewajs**[4], **Steven G. DuBois**[4], **Katherine K. Matthay**[4], and **Youngho Seo**[1,5,6]

[1]Department of Radiology and Biomedical Imaging, University of California, San Francisco, California [2]J. Grayton Pruitt Family Department of Biomedical Engineering, University of Florida, Gainesville, Florida [3]Division of Cancer Epidemiology and Genetics, National Cancer Institute, National Institutes of Health, Bethesda, Maryland [4]Department of Pediatrics, UCSF School of Medicine and UCSF Benioff Children's Hospital, San Francisco, California [5]Department of Radiation Oncology, University of California, San Francisco, California [6]Joint Graduate Group in Bioengineering, University of California, San Francisco and Berkeley, California

Abstract

Purpose—Iodine-131-m-iodobenzylguanidine ([^{131}I]mIBG) targeted radionuclide therapy (TRT) is a standard treatment for recurrent or refractory neuroblastoma with response rates of 30–40%. The aim of this study is to demonstrate patient-specific dosimetry using quantitative [^{124}I]mIBG PET/CT imaging with a Geant4-based Monte Carlo method for better treatment planning.

Procedures—A Monte Carlo dosimetry method was developed using the Geant4 toolkit with voxelized anatomical geometry and source distribution as input. The pre-segmented hybrid computational human phantoms developed by the University of Florida and the National Cancer Institute (UF/NCI) were used as a surrogate to characterize the anatomy of a given patient. S-values for I-131 were estimated by the phantoms coupled with Geant4 and compared with those estimated by OLINDA|EXM and MCNPX for the newborn model. To obtain patient-specific biodistribution of [^{131}I]mIBG, a 10-year-old girl with relapsed neuroblastoma was imaged with [^{124}I]mIBG PET/CT at four time points prior to the planned [^{131}I]mIBG TRT. The organ and tumor absorbed dose of the clinical case were estimated with the Geant4 method using the modified UF/NCI 10-year-old phantom with tumors and the patient-specific residence time.

Corresponding author: Shih-ying Huang, Department of Radiology and Biomedical Imaging, University of California, San Francisco, California 94143-0946. Shih-ying.Huang@ucsf.edu.

Conflict of Interest

The authors declare that they have no conflict of interest.

Results—For the newborn model, the Geant4 S-values were consistent with the MCNPX S-values. The S-value ratio of the Geant4 method to OLINDA|EXM ranged from 0.08 to 6.5 of all major organs. The [^{131}I]mIBG residence time quantified from the pretherapy [^{124}I]mIBG PET/CT imaging of the 10-year-old patient was mostly comparable to those previously reported. Organ absorbed dose for the salivary glands were 98.0 Gy, heart wall, 36.5 Gy, and liver, 34.3 Gy; while tumor absorbed dose ranged from 143.9 Gy to 1641.3 Gy in different sites.

Conclusions—Patient-specific dosimetry for [^{131}I]mIBG targeted radionuclide therapy was accomplished using pretherapy [^{124}I]mIBG PET/CT imaging and a Geant4-based Monte Carlo dosimetry method. The Geant4 method with quantitative pretherapy imaging can provide dose estimates to normal organs and tumors with more realistic simulation geometry, and thus may improve treatment planning for [^{131}I]mIBG TRT.

Keywords

neuroblastoma; [^{131}I]-m-iodobenzylguanidine; targeted radionuclide therapy; [^{124}I]mIBG PET/CT imaging; dosimetry; Monte Carlo simulation

Introduction

Neuroblastoma is a neuroendocrine tumor of children derived from neural crest in the sympathetic nervous system. Half of neuroblastoma cases are metastatic at diagnosis, with a long-term survival rate less than 40% with intensive multimodality therapy including chemotherapy induction, surgery, radiotherapy, myeloablative treatment, and therapy for minimal residual disease [1–3]. Iodine-131-m-iodobenzylguanidine ([^{131}I]mIBG) was introduced as another approach to treat neuroblastoma with targeted radionuclide therapy (TRT). Since mIBG has a similar transport mechanism to norepinephrine, 90% percent of neuroblastoma is mIBG avid [4,5]. [^{131}I]MIBG TRT has become a standard treatment approach for recurrent or refractory cases of neuroblastoma with response rates of 20% – 37% [2,3,6–8].

Currently, [^{131}I]mIBG TRT treatment planning has been based on the maximum tolerable dose per patient's body weight, and internal dosimetry from the treatment has been approximated with planar imaging and OLINDA|EXM. While OLINDA|EXM is a useful tool for internal dosimetry, several studies [9–12] have reported that the stylized phantoms [13] built into OLINDA|EXM (version 1.1) and realistic voxel phantoms yields a dose discrepancy, which may be pertinent to address for therapy planning. Recent efforts have been made in updating radiation dosimetry in OLINDA by considering realistic voxelized reference human phantoms. Since dosimetry for [^{131}I]mIBG TRT has been challenging, we proposed the use of [^{124}I]mIBG dynamic PET/CT imaging to evaluate patient-specific dosimetry prior to [^{131}I]mIBG TRT. The [^{131}I]mIBG biodistribution quantified from [^{124}I]mIBG PET imaging is assumed to be a reasonable approach with closer half-life of I-124 (4.18 days) and I-131 (8.02 days). Accurate dosimetry from whole-body [^{131}I]MIBG SPECT/CT imaging may be limited due to difficult image quantification. Despite the lower positron yield, scattered radiation, and cascaded emissions from I-124, [^{124}I]mIBG PET/CT imaging is more suitable for whole-body imaging with reasonable image quantification for diagnostic and dosimetry purposes. The [^{131}I]mIBG biodistribution quantified by pretherapy

[^{124}I]mIBG PET/CT imaging in murine models [14–16] has been shown to be helpful to estimate radiation dose.

In this study, a Geant4 (GEometry ANd Tracking 4) [17,18] Monte Carlo method was investigated for use with [^{124}I]mIBG pretherapy PET/CT imaging to estimate radiation dose close to patient-specific dosimetry. Dose estimates from the Geant4 dosimetry method, OLINDA|EXM [19], and the data published by Wayson, *et al.* [20] using MCNPX were compared. In addition, we show an example of using the Geant4 method with a clinical dataset of a patient imaged with [^{124}I]mIBG PET/CT prior to [^{131}I]mIBG TRT.

Materials and Methods

Computational Human Phantoms

Non-uniform rational B-spline (NURBS) hybrid computational phantoms developed by the University of Florida (UF) and the National Cancer Institute (NCI) [21,22] were used to describe human anatomy in the Monte Carlo simulation. The UF/NCI phantoms define 126 anatomical organ and tissue models including 38 skeletal sites. The UF/NCI newborn and 10-year-old female phantoms were used to define anatomical geometry realistic to the human in the simulation because organs and tissues are already segmented in the UF/NCI phantoms, which will substantially eliminate the time for segmenting the CT images. Tissue composition and density of the UF/NCI phantoms were defined according to Lee et al, 2007 [21]. The UF/NCI phantoms were generated with an isotropic voxel resolution of 1.0 mm^3.

Internal Dosimetry Approach

Internal dosimetry was estimated according to the Medical Internal Radiation Dose (MIRD) system [23]. For a given radionuclide, S-value (mGy/MBq-s) is defined as the dose factor from a source organ (r_S) to a target organ (r_T) as follows,

$$S(r_T \leftarrow r_S) = \frac{k \sum_i y_i E \phi_i(r_T \leftarrow r_S)}{m_{r_T}} \quad \text{(eq. 1)}$$

where E is the energy per radiation (MeV), y_i is the number of radiations with energy E_i emitted per nuclear transition, $\varphi_i(r_T \leftarrow r_S)$ is the fraction of energy emitted that is absorbed in the target, k is a constant (Gy-kg/MBq-s-MeV), and m_{r_T} is the mass of target region. For all nonskeletal source and target organs, S-values of a given radionuclide were calculated using the eq. 1. For the skeletal target tissues, dose enhancement from photons to S-value $S_{photon}(r_T \leftarrow r_S)$ was estimated using the skeletal photon dose response function (DRF) precalculated for the UF/NCI phantoms [24] as follows,

$$S_{photon}(r_T \leftarrow r_S) = k \sum_j w_j(r_T) \sum_i \left[\frac{D(r_T)}{F(E_i)}\right] F(j \leftarrow r_S; E_i) \quad \text{(eq. 2)}$$

where $w_j(r_T)$ is the mass fraction of the target tissue r_T in bone site j, $D(r_T)/F(E_i)$ is the skeletal photon DRF for the target tissue r_T at photon energy E_i, $F(j \leftarrow r_S; E_i)$ is the photon flux emitted from the source organ r_S incident on the spongiosa or medullary cavity of the

bone site *j* for photon energy E_i. The mass fraction of the skeletal tissues reported for the UF/NCI newborn phantom [25] was used for S-value to skeletal target tissue. Since photons or gamma rays emitted from any organ are the predominant particles depositing dose in the skeletal tissues, $S(r_T \leftarrow r_S) \approx S_{photon}(r_T \leftarrow r_S)$ was assumed for all nonskeletal source organs to skeletal target tissues.

For skeletal source tissues, the dose enhancement in the S-value from electrons $S_{electron}(r_T \leftarrow r_S)$ was computed as,

$$S_{electron}(r_T \leftarrow r_S) = \sum_i N(E_i)\Phi(r_T \leftarrow r_S; E_i) \quad \text{(eq. 3)}$$

where $N(E_i)$ is the number of electrons emitting from the skeletal source tissue and $\Phi(j \leftarrow r_S; E_i)$ is the skeletal-averaged electron specific absorbed fraction (g^{-1}). $\Phi(j \leftarrow r_S; E_i)$ precalculated for the UF/NCI newborn phantom [26] was used to estimate the S-value. Since dose contribution from electrons and photons were considered for all skeletal source tissues to skeletal target tissues, $S(r_T \leftarrow r_S) = S_{photon}(r_T \leftarrow r_S) = + S_{electron}(r_T \leftarrow r_S)$ was assumed. Due to unavailable skeletal-averaged electron specific absorbed fraction for the 10-year-old phantom and bone marrow mass, the skeletal dosimetry in the UF/NCI 10-year-old phantom was approximated by considering dose enhancement from only photons. The mass of active marrow of the UF/NCI 10-year-old phantom was approximated by the mass proportion reported Table I of Xie *et al.*, 2013 [27].

Monte Carlo Particle Transport

An internal dosimetry tool was developed using the Geant4 Monte Carlo particle transport toolkit (version 4.9.6.p02). The dosimetry tool allows flexible definition of geometry and source distribution. *G4VNestedParameterization* was implemented to enable voxelized geometry definition in the simulation geometry with efficient particle transport. The user-defined primary source distribution was implemented in the *G4UserPrimaryGenerator* to randomly sample primary source position based on a given probability distribution. The primary source was uniformly distributed in a given organ with isotropic angular momentum. Geant4 modular physics lists including *G4RadioActiveDecayPhysics*, *G4DecayPhysics*, and *G4EmStandardPhysics_option4* were enabled to simulate the radioactive decay processes and physics processes in the low energy regime. The radioactive decay products were sampled based on the ENSDF (Evaluated Nuclear Structure Data File) data library [28]. A three-body decay algorithm was used to sample the β-decay spectrum [29]. A range cut-off of 0.1-mm was set for all particles. In order to compute S-values appropriately, three derived classes of *G4VPrimitiveScorer* via *G4MultiFunctionalDetector* were constructed to score the following hit information in the voxelized geometry: the total energy deposit (MeV), the photon flux (cm^{-2}) per energy bin, and the energy histogram of electrons in the source tissue.

Ten million and twenty million histories in each source organ were simulated for the newborn and the 10-year-old phantoms, respectively. All simulations were performed on a Relion 2800GT server (Penguin Computing, Fremont, CA) with sixteen 2.7-GHz Intel Xeon E5-2680 cores and 256 GB of available memory. Monte Carlo simulations were performed

in 10 batches of 10-million or 20-million histories. Each batch was initialized with a different random number seed. The coefficient of variation (CV) was expressed as a percentage of the mean of the 10 S-values measured for each source organ.

For benchmarking purposes, the Geant4 S-values computed for the UF/NCI newborn phantom were cross-checked with those computed with Monte Carlo N-Particle eXtended (MCNPX) in Wayson *et al*., 2010 [20]. In addition, Geant4-S-values were compared with the mass-adjusted S-values from OLINDA|EXM (version 1.1) for the newborn and the 10-year-old models. Due to the different skeletal dosimetry approach used in this study, the mass of red marrow and osteogenic cells was not modified in OLINDA for the Geant4 and OLINDA comparison.

Acquisition and Quantification of [^{124}I]MIBG PET/CT Imaging

At UCSF, one case of [^{124}I]mIBG pretherapy imaging was performed in 2013 for a 10-year-old female patient with relapsed neuroblastoma. The patient recruitment and procedures followed a protocol approved by the UCSF Committee on Human Research and FDA IND (#113907) and appropriate informed consent was obtained. No-carrier-added [^{124}I]mIBG (0.695 mCi) was prepared as previously reported [14], and was administered intravenously, with potassium iodide administered orally for thyroid protection. The patient was imaged with a PET/CT system (Discovery VCT, GE Healthcare, Waukesha, WI) at 4 time points (1.5 hr, 19.5 hr, 43.5 hr, and 115 hr after [^{124}I]MIBG injection). The [^{124}I]mIBG whole-body PET images were acquired in 3D mode with 4-min per bed for the first 3 time points and 5-min per bed for the last day of imaging using an energy window between 425 keV and 650 keV. For image post-processing, the random events were corrected by a singles-based method, and a model-based algorithm was used to correct the scattered events. A filtered backprojection algorithm provided by the manufacturer was used to reconstruct the CT images with a voxel size of 1.4×1.4×5.0 mm^3 for attenuation correction. The PET images were reconstructed using an ordered subsets expectation maximization algorithm (14 subsets and 4 iterations) provided by the scanner manufacturer with a 9-mm Gaussian postfilter (voxel size of 5.5×5.5×3.3 mm^3). The manufacturer-provided PET reconstruction algorithm did not include a resolution recovery model. For all source organs, volumes of interest (VOIs) were drawn manually on the CT images using AMIDE (version 1.0.1) [30] over the entire organ. For tumors, VOIs larger than the entire tumor activity volume excluding the background activities were contoured using PMOD (PMOD Technologies Ltd) to reduce the partial volume effect. The total [^{124}I]mIBG uptake of the organ and tumor VOIs in the PET images were calculated. All remaining activities were uniformly distributed in the remaining body. Since appropriate I-124 decay correction was not implemented for PET reconstruction, total whole-body uptake quantified from [^{124}I]mIBG PET images was decay-corrected at each time point as a reference to calculate percent injected activity (%IA). Considering excretion of [^{124}I]mIBG, the decay-corrected [^{124}I]mIBG time activity curves (TACs) were fitted with a bi-exponential function to estimate [^{131}I]mIBG residence times analytically. The patient had a prior left adrenalectomy for treatment of her primary neuroblastoma, thus compensatory uptake of [^{124}I]MIBG was observed in the contralateral adrenal gland in the [^{124}I]mIBG PET images at the later time points. However, the time activity curve quantified for the right adrenal gland was insufficient to accurately estimate

the [^{131}I]mIBG residence time of the adrenal gland. Thus, the adrenal uptake of [^{131}I]mIBG was excluded for the final dose estimate. The patient was treated with 18 mCi/kg [^{131}I]MIBG 8 days after [^{124}I]MIBG injection (patient weight: 29 kg). A standard dose of [^{131}I]mIBG was delivered and not adjusted based upon results of the [^{124}I]mIBG research imaging.

Patient-Specific Geant4-based Dosimetry using [^{124}I]mIBG PET/CT Imaging

To estimate patient-specific dosimetry, the UF/NCI 10-year-old female phantom was used for its body size and anatomy, similar to those of the clinical case. Source organs identified in the [^{124}I]mIBG PET images of the clinical case include urinary bladder, brain, liver, lungs, salivary glands, spleen, and thyroid. In addition, 12 lesions were identified in the patient and were contoured using PMOD. All lesions were bone metastases, and CT images could not determine a meaningful tumor volume. Thus, tumor volume was approximated by the metabolic tumor volume [31] using the [^{124}I]mIBG PET images. The metabolic tumor volume was defined as the volume of hypermetabolic tissue with a threshold of greater than 50% of the maximum uptake in the entire tumor site. We used the threshold of 50% of the maximum uptake following a phantom study in Ciernick et al. [32]. The metabolic tumor volumes were then carefully placed in the UF/NCI 10-year-old phantom as close as possible to the tumor location in the clinical case. The modified UF/NCI 10-year-old phantom was the input geometry to the Geant4 method with [^{131}I]mIBG uniformly distributed in all source organs and tumors identified in the [^{124}I]mIBG PET images. For the Monte Carlo simulations, water was assumed to characterize tumor composition and density. The S-values of all source and target organs were calculated for dose estimate. Total absorbed dose D_{r_T} to a target organ r_T were computed as the following,

$$D_{r_T} = A_0 \sum_i \tilde{A}_{r_i} \cdot S(r_T \leftarrow r_i) \quad \text{(eq. 4)}$$

where A_0 is the initial injected activity and $\tilde{A}_{r_i}$ is the [^{131}I]mIBG residence time (MBq-hr/MBq) of a source organ r_i. The total absorbed dose estimated from the Geant4 method was reported for normal organs and tumors. The portion of total absorbed dose from cross-irradiation and self-irradiation was evaluated for all tumors.

Results

For one source organ, the average time of the I-131 Monte Carlo simulations was 5.2 hr (10-million events) and 19.5 hr (20-million events) for UF/NCI newborn phantom and UF/NCI 10-year-old phantom, respectively.

Benchmark of S-values Between MCNPX and Geant4

The S-values of the Geant4 dosimetry method were benchmarked with those simulated with the same UF/NCI newborn phantom in Wayson et al., 2010 [20] using MCNPX. For the adrenal source in the UF/NCI newborn phantom, Figure 1 shows that the Geant4 S-values consistently agree with the MCNPX S-values. The S-value ratio of Geant4 to MCNPX was close to unity ranging from 0.90 to 1.1. Supplemental Table 1 shows consistent agreement in the newborn S-values between Geant4 and MCNPX with a ratio ranged between 0.23 and

1.13 for non-skeletal organs while some discrepancies were observed in the hollow organs and skeletal tissues.

S-value Comparison Between OLINDA|EXM and Geant4

The S-value differences between the Geant4 dosimetry method and OLINDA were examined. For the adrenal source in the newborn model, the mean S-value (± standard deviation, mGy/MBq-s) computed by Geant4 and OLINDA is compared in Figure 2. The Geant4 method suggests that the self-irradiation dose was 97.3% (OLINDA: 98.1%) of total organ dose while the cross-irradiation dose to other organs ranged from 0.09% to 0.46% of total organ dose (OLINDA: 0.06% to 0.35%). The S-value ratio of Geant4 to OLINDA ranges between 0.59 (heart wall target) and 2.4 (stomach wall target). For all major organs in the newborn and the 10-year-old models, supplemental Table 2 – 4 show the self-irradiation S-values were consistent between Geant4 and OLINDA while differences were found for small organs and between organs that are anatomically distant, which give rise to larger S-values CV. Figure 4 shows a visual comparison of the anatomy modeled in the Geant4 method and OLINDA with the clinical CT images. Supplemental Figure 1 and Figure 2 show that the large difference in the organ contour and positions between the UF/NCI and the stylized phantoms resulted in nonnegligible S-value discrepancy.

Patient-Specific Dosimetry Estimation Using [^{124}I]mIBG PET/CT

The clinical efficacy of the patient-specific pretherapy dosimetry planning of [^{131}I]mIBG TRT was examined by considering [^{131}I]mIBG biodistribution estimated from the [^{124}I]mIBG PET/CT imaging using the Geant4 dosimetry method. Figure 3 shows the coronal slices of [^{124}I]mIBG PET/CT registered images at 4 time points. Figure 4 illustrates the VOIs of lesion #2 contoured for the [^{124}I]mIBG uptake quantification and the metabolic tumor volume on the clinical [^{124}I]mIBG PET/CT images and on the UF/NCI 10-yr-old phantom closely registered to the PET/CT images. Figure 5 illustrates the TACs with the fitted bi-exponential functions for source organs of brain, heart, salivary glands, spleen, thyroid, liver, lungs, and some lesions. The [^{131}I]mIBG residence times estimated from the [^{124}I]MIBG TACs in all major organs except the heart, the thyroid, and the liver were found to be within the range of those estimated in the previous studies in Table 1. Figure 6 identifies the location of the lesions found in the patient based on the pretherapy [^{124}I]mIBG PET images acquired at the last time point. Table 2 shows the [^{131}I]mIBG tumor residence time with the corresponding metabolic tumor volume. The highest [^{131}I]mIBG residence time was found in lesion #2, which had the largest metabolic tumor volume.

Considering the patient-specific [^{131}I]mIBG residence time in Table 1 and Table 2 and the injected activity of [^{131}I]mIBG TRT, the patient received absorbed dose larger than 10 Gy to spleen (16.0 Gy), lungs (21.2 Gy), thyroid (22.6 Gy), liver (34.3 Gy), heart wall (36.5 Gy), and salivary glands (98.0 Gy). The absorbed dose in tumors ranged from 143.9 Gy to 1641.3 Gy with larger absorbed dose delivered to tumors with a smaller metabolic tumor volume, such as lesion #3 and #4. Lesion #9 and #10 received more than 1% of the total organ dose from cross-irradiation of the surrounding organs. Tables 2 and 3 summarize the absorbed dose estimated by this dosimetry method to the patient's normal organs and tumors.

Discussion

A dosimetry approach of [^{131}I]mIBG TRT was introduced by using patient-specific residence time quantified from pretherapy [^{124}I]mIBG PET/CT imaging and realistic anatomy in the Monte Carlo simulations. Overall, the S-values from the Geant4 method were similar to the OLINDA S-values for self-irradiation while some discrepancy was observed for cross-irradiation, especially among distant and smaller organs. Consistent agreement in S-values between Geant4 and MCNPX confirms the integrity of the Geant4 method using the same UF/NCI newborn phantoms. This study also shows that this dosimetry method is feasible to estimate absorbed dose to normal organs and tumors close to those specific to a given patient. In addition, the Geant4 method has full freedom in modeling the clinical environment realistic to a patient, such as lesion location and detailed particle information.

There are several factors to consider when comparing the dosimetry result between the Geant4 method and OLINDA|EXM or MCNPX. The S-values from the Geant4 dosimetry method were estimated with the UF/NCI phantoms, which is anatomically different from Cristy and Eckerman stylized phantoms [13] used in OLINDA|EXM. The S-value discrepancy between Geant4 and OLINDA in this study is mainly due to the difference in human anatomy and contour defined in the Monte Carlo particle transport. The distance and contour in the stylized phantoms is quite different from that in the UF/NCI phantoms, which represent more realistic human anatomy. Supplementary Figure 1 shows that the large S-value difference between the Geant4 method and OLINDA to the thymus source organ could likely due to very different organ position and contour between the UF/NCI phantom and the stylized phantom. It also shows that the UF/NCI phantom provided human anatomy more realistic to the clinical CT images, which could improve the accuracy of the dose estimate. Supplementary Figure 2 suggests that difference in inter-organ distance modeled in the UF/NCI and the stylized phantoms can contribute to the S-value difference between the Geant4 method and OLINDA. For example, the stylized newborn phantom modeled the stomach by an ellipsoid shape with a gap from the kidney approximately 17-mm larger than that in the UF/NCI phantom with more realistic organ contour. Different particle transport methods could contribute to the S-value difference between OLINDA and Geant4. OLINDA used the ALGAMP Monte Carlo code [33] by tracking electrons and photons separately to obtain monoenergetic specific absorbed fractions while radioactive decay products were directly simulated in the Geant4 method. OLINDA used a skeletal dosimetry model that assumed the skeletal dose response function for all the bone sites can be simply represented by those of parietal bone and lumbar vertebra [13]. On the contrary, the UF/NCI phantoms were developed with a detailed skeletal dosimetry model that computed skeletal dose response function 40 bone sites based on microCT images of the bone sites. For the wall or content of hollow organs, the S-value difference between Geant4 and OLINDA or MCNPX may be attributed to the analytical definition of S-values from content to wall [34] in OLINDA and the variance reduction techniques implemented in the MCNPX method. Other factors such as tissue composition, density, and Monte Carlo transport physics of photons and electrons for the energy range of interest can contribute the S-value difference between Geant4 and other methods.

The pretherapy [^{124}I]mIBG PET/CT imaging of the 10-year-old patient serves as a good example to evaluate the efficacy of the Geant4 dosimetry method for more realistic dosimetry planning in a clinical setting. The UF/NCI hybrid computation phantoms include a family of human phantoms with various age and body size [35], thus, one can select a UF/NCI phantom that best resembles the anatomy of a given patient as the input to the Geant4 dosimetry tool. This approach eliminates the time spent to segment or contour organs of interest on the CT images for the geometry input to the Geant4 method. The process of outlining organs or volume of interest may be time-prohibitive and error-prone especially with low-dose CT images for PET attenuation correction, not to mention the uncertainty introduced in estimating the material density from the CT Hounsfield units. Furthermore, one can modify the UF/NCI phantoms by incorporating realistic tumor volumes at any given location. Any radionuclide can be simulated for a given source distribution such as non-uniform distribution. Thus, the dosimetry may be estimated with this flexible Geant4 method and not limited by capability of existing dosimetry software. For example, [^{124}I]mIBG PET images of the patient indicated some mIBG uptake in the salivary glands. S-values of salivary glands were not available in OLINDA, which may neglect considerable absorbed dose to salivary glands (Table 3). In addition to the flexible dosimetry method, [^{124}I]mIBG PET/CT imaging is helpful to achieve more realistic dosimetry planning prior to [^{131}I]mIBG TRT. This study shows that the [^{124}I]mIBG PET/CT imaging at UCSF effectively quantified the patient-specific [^{124}I]mIBG residence time. The [^{131}I]mIBG residence times estimated from the [^{124}I]mIBG PET images were comparable to those observed in adult human and murine studies for most organs. Abnormal uptake of [^{124}I]mIBG may exist in the liver, which could cause the higher [^{131}I]mIBG residence time for this clinical case (Table 1) compared to those reported in the past studies. The small study sample size and the different thyroid blocking methods could contribute to the deviation in residence time of the heart and the thyroid estimated in this study. In this study, the patient-specific dosimetry was referred to the dose estimated with the Geant4 method considering a realistic human anatomy and patient-specific residence time quantified from the [^{124}I]mIBG PET imaging. The absorbed dose can help optimize the [^{131}I]mIBG TRT by considering toxicity to dose-limiting organs such as bone marrow and liver. For this clinical case, self-irradiation mainly contributed to the absorbed dose of tumors that were distant from other source organs. While tumor self-irradiation dose may be a good assumption, this study estimated some cross-irradiation from the lung source contributing to lesion #9 and #10 located close to the lungs. Though the % cross-irradiation of these lesions is less than 5%, the residence time and the location of tumor to other source organs could affect the absorbed dose to tumors in ways that might not be addressed simply by the self-irradiating sphere model. Matthay et al. [36] reported similar tumor absorbed dose ranged from 31.2 Gy to 3050 Gy from a cohort who received a median [^{131}I]mIBG activity of 15 mCi/kg using conjugate planar imaging and OLINDA|EXM. Furthermore, the patient-specific TACs and 3D dose distribution of organs and tumors may be helpful to further optimize the treatment planning.

There are limitations to consider in this study. The assumptions made in calculating skeletal dosimetry of the UF/NCI 10-year-old phantom may introduce uncertainty in the S-value from the skeletal source or target tissue, which was included in the S-value of total body as a

source or target organ. Since the [^{131}I]mIBG residence time of the remainder body was high among other source organs in this study, the uncertainty from the skeletal dosimetry may contribute error in the final absorbed dose. The accuracy of total [^{131}I]mIBG uptake quantified by the PET images may be affected by the contoured VOIs and partial volume effect in the reconstructed PET images. Although the modified UF/NCI phantoms are helpful in defining realistic geometry in the Monte Carlo simulations for much improved dose estimate, the absorbed dose was not truly patient-specific because the UF/NCI phantoms and the patient anatomy are not identical. Comparison of the dose estimate between the UF/NCI phantoms and the clinical CT images will be investigated in the future studies.

Conclusion

This study demonstrated the feasibility of estimating patient-specific dosimetry of [^{131}I]mIBG targeted radionuclide therapy using pretherapy [^{124}I]mIBG PET/CT imaging. Instead of assuming the [^{131}I]mIBG residence time determined in the past studies or approximated by planer imaging, this study shows that [^{124}I]mIBG PET pretherapy imaging was clinically feasible to predict patient-specific [^{131}I]mIBG residence time of normal organs and tumors. In addition, a Geant4 dosimetry method has been developed to use with the patient-specific residence time. The flexible Geant4 method can tailor Monte Carlo simulations to realistic anatomy and source distribution for estimating organ and tumor dosimetry to correlate with treatment response. With the ever-improving hardware and software advancement and clinically streamlined workflow, the Monte-Carlo-based dosimetry method with pretherapy [^{124}I]mIBG PET/CT imaging may be feasible in a clinical setting.

Supplementary Material

Refer to Web version on PubMed Central for supplementary material.

Acknowledgments

The authors would like to thank the clinical coordinators, technologists, nurses, and physicians who made this study possible at UCSF. We also would like to thank Jungwook Shin, Ph.D. for helpful advice for developing Geant4 simulations. This work was supported in part by the National Cancer Institute under grants R01 CA154561 and P01 081403 and by the Alex's Lemonade Stand and Dougherty Foundations.

References

1. Matthay KK, Tan JC, Villablanca JG, et al. Phase I dose escalation of iodine-131-metaiodobenzylguanidine with myeloablative chemotherapy and autologous stem-cell transplantation in refractory neuroblastoma: a new approaches to Neuroblastoma Therapy Consortium Study. J Clin Oncol. 2006; 24:500–506. [PubMed: 16421427]
2. Matthay KK, Weiss B, Villablanca JG, et al. Dose escalation study of no-carrier-added 131I-metaiodobenzylguanidine for relapsed or refractory neuroblastoma: new approaches to neuroblastoma therapy consortium trial. J Nucl Med. 2012; 53:1155–1163. [PubMed: 22700000]
3. Matthay KK, Yanik G, Messina J, et al. Phase II study on the effect of disease sites, age, and prior therapy on response to iodine-131-metaiodobenzylguanidine therapy in refractory neuroblastoma. J Clin Oncol. 2007; 25:1054–1060. [PubMed: 17369569]

4. Carlin S, Mairs RJ, McCluskey AG, et al. Development of a real-time polymerase chain reaction assay for prediction of the uptake of meta-[(131)I]iodobenzylguanidine by neuroblastoma tumors. Clin Cancer Res. 2003; 9:3338–3344. [PubMed: 12960120]
5. Treuner J, Feine U, Niethammer D, et al. Scintigraphic imaging of neuroblastoma with [131-I]iodobenzylguanidine. Lancet. 1984; 1:333–334. [PubMed: 6141395]
6. Matthay KK, DeSantes K, Hasegawa B, et al. Phase I dose escalation of 131I-metaiodobenzylguanidine with autologous bone marrow support in refractory neuroblastoma. J Clin Oncol. 1998; 16:229–236. [PubMed: 9440747]
7. DuBois SG, Matthay KK. 131I-Metaiodobenzylguanidine therapy in children with advanced neuroblastoma. Q J Nucl Med Mol Im. 2013; 57:53–65.
8. Wilson JS, Gains JE, Moroz V, Wheatley K, Gaze MN. A systematic review of I-meta iodobenzylguanidine molecular radiotherapy for neuroblastoma. Eur J Cancer. 2013
9. Yoriyaz H, Stabin MG, dos Santos A. Monte Carlo MCNP-4B-based absorbed dose distribution estimates for patient-specific dosimetry. J Nucl Med. 2001; 42:662–669. [PubMed: 11337557]
10. Stabin MG, Yoriyaz H. Photon specific absorbed fractions calculated in the trunk of an adult male voxel-based phantom. Health Phys. 2002; 82:21–44. [PubMed: 11768796]
11. Lee C, Park S, Lee JK. Specific absorbed fraction for Korean adult voxel phantom from internal photon source. Radiat Prot Dosimet. 2007; 123:360–368.
12. Lamart S, Bouville A, Simon SL, et al. Comparison of internal dosimetry factors for three classes of adult computational phantoms with emphasis on I-131 in the thyroid. Phys Med Biol. 2011; 56:7317–7335. [PubMed: 22040775]
13. Cristy, M.; Eckerman, KF. Specific Absorbed Fractions of Energy at Various Ages from Internal Photon Sources: 1, Methods. Oak Ridge, TN: Oak Ridge National Laboratory; 1987.
14. Lee C-L, Wahnishe H, Sayre GA, et al. Radiation dose estimation using preclinical imaging with 124I-metaiodobenzylguanidine (MIBG) PET. Med Phys. 2010; 37:4861. [PubMed: 20964203]
15. Seo Y, Gustafson WC, Dannoon SF, et al. Tumor Dosimetry Using [124I]m-iodobenzylguanidine MicroPET/CT for [131I]m-iodobenzylguanidine Treatment of Neuroblastoma in a Murine Xenograft Model. Mol Imag Biol. 2012; 14:735–742.
16. Moroz MA, Serganova I, Zanzonico P, et al. Imaging hNET reporter gene expression with 124I-MIBG. J Nucl Med. 2007; 48:827–836. [PubMed: 17475971]
17. Agostinelli S, Allison J, Amako K, et al. Geant4—a simulation toolkit. Nucl Instrum Methods Phys Res A. 2003; 506:250–303.
18. Allison J, Amako K, Apostolakis J, et al. Geant4 developments and applications. IEEE Trans Nucl Sci. 2006; 53:270–278.
19. Stabin MG, Sparks RB, Crowe E. OLINDA/EXM: the second-generation personal computer software for internal dose assessment in nuclear medicine. J Nucl Med. 2005; 46:1023–1027. [PubMed: 15937315]
20. Wayson M, Lee C, Sgouros G, et al. Internal photon and electron dosimetry of the newborn patient--a hybrid computational phantom study. Phys Med Biol. 2012; 57:1433–1457. [PubMed: 22354044]
21. Lee C, Lodwick D, Hasenauer D, Williams JL, Bolch WE. Hybrid computational phantoms of the male and female newborn patient: NURBS-based whole-body models. Phys Med Biol. 2007; 52:3309–3333. [PubMed: 17664546]
22. Lee C, Lodwick D, Hurtado J, et al. The UF family of reference hybrid phantoms for computational radiation dosimetry. Phys Med Biol. 2010; 55:339–363. [PubMed: 20019401]
23. Loevinger, R.; Budinger, TF.; Watson, EE. MIRD primer for absorbed dose calculations. New York: Society of Nuclear Medicine; 1988.
24. Johnson PB, Bahadori AA, Eckerman KF, Lee C, Bolch WE. Response functions for computing absorbed dose to skeletal tissues from photon irradiation--an update. Phys Med Biol. 2011; 56:2347–2365. [PubMed: 21427484]
25. Pafundi D, Lee C, Watchman C, et al. An image-based skeletal tissue model for the ICRP reference newborn. Phys Med Biol. 2009; 54:4497–4531. [PubMed: 19556686]

26. Pafundi D, Rajon D, Jokisch D, Lee C, Bolch W. An image-based skeletal dosimetry model for the ICRP reference newborn--internal electron sources. Phys Med Biol. 2010; 55:1785–1814. [PubMed: 20208096]
27. Xie T, Bolch WE, Lee C, Zaidi H. Pediatric radiation dosimetry for positron-emitting radionuclides using anthropomorphic phantoms. Med Phys. 2013; 40:102502. [PubMed: 24089923]
28. Tuli, J. Evaluated Nuclear Structure Data File (ENSDF) Retrieval. 2014. <http://www.nndc.bnl.gov/ensdf/>.
29. Hauf S, Kuster M, Batic M, et al. Radioactive decays in Geant4. 2013
30. Loening AM, Gambhir SS. AMIDE: a free software tool for multimodality medical image analysis. Molecular imaging. 2003; 2:131–137. [PubMed: 14649056]
31. Bazan JG, Koong AC, Kapp DS, et al. Metabolic tumor volume predicts disease progression and survival in patients with squamous cell carcinoma of the anal canal. J Nucl Med. 2013; 54:27–32. [PubMed: 23236018]
32. Ciernik IF, Dizendorf E, Baumert BG, et al. Radiation treatment planning with an integrated positron emission and computer tomography (PET/CT): A feasibility study. Int J Radiat Oncol Biol Phys. 2003; 57:853–863. [PubMed: 14529793]
33. Evans JF, Stabin MG, Stubbs JB. Specific absorbed fractions of energy from internal photon sources in brain tumor and cerebrospinal fluid. Med Phys. 1995; 22:331–340. [PubMed: 7596323]
34. Stabin MG, Siegel JA. Physical models and dose factors for use in internal dose assessment. Health Phys. 2003; 85:294–310. [PubMed: 12938720]
35. Johnson PB, Whalen SR, Wayson M, et al. Hybrid Patient-Dependent Phantoms Covering Statistical Distributions of Body Morphometry in the US Adult and Pediatric Population. Proc IEEE. 2009; 97:2060–2075.
36. Matthay KK, Panina C, Huberty J, et al. Correlation of tumor and whole-body dosimetry with tumor response and toxicity in refractory neuroblastoma treated with 131I-MIBG. J Nucl Med. 2001; 42:1713–1721. [PubMed: 11696644]

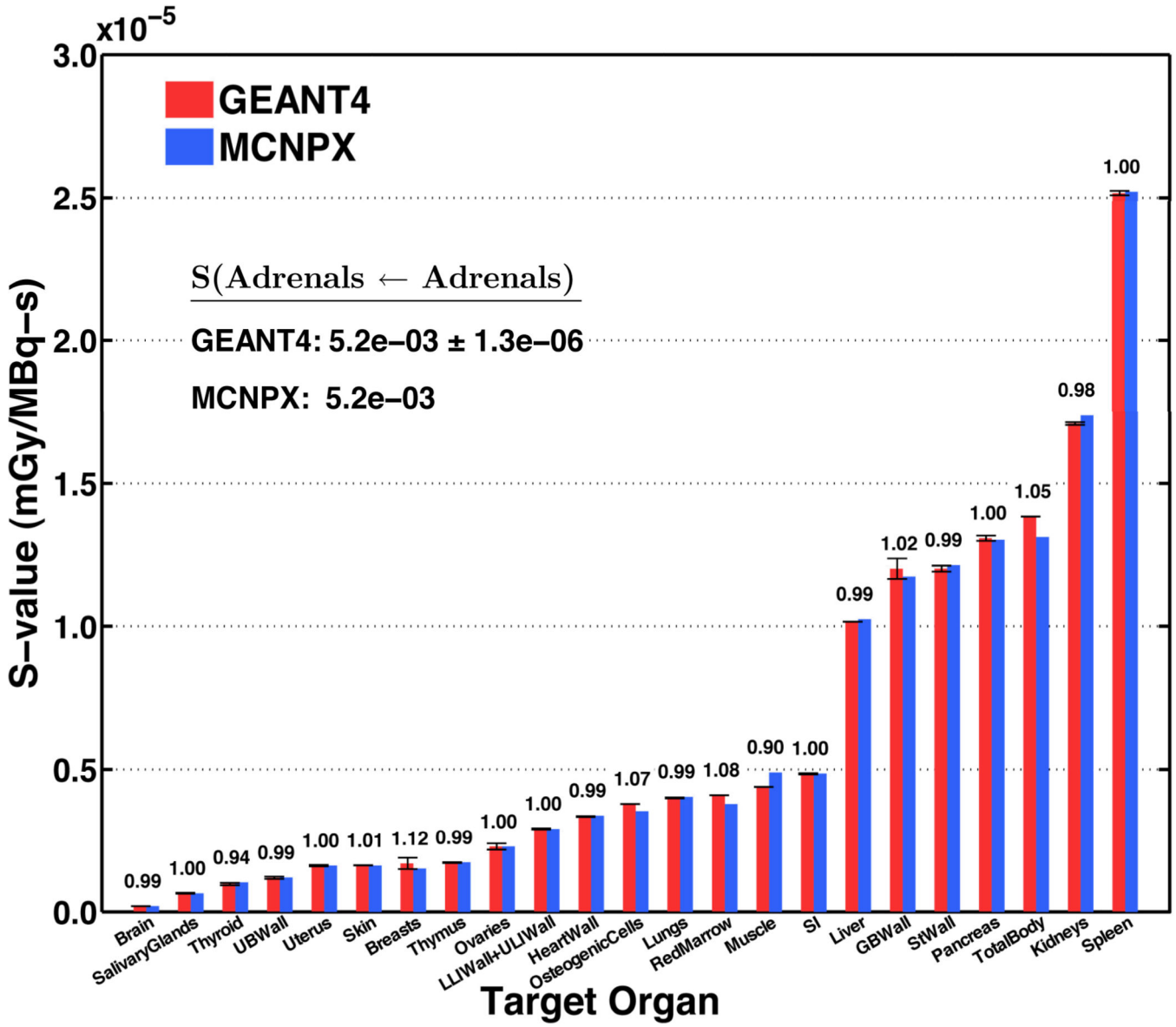

Figure 1.

The comparison of the I-131 S-value (mGy/MBq-s) ± standard deviation for the newborn model between the Geant4 method (left red bar) and the MCNPX method (right blue bar) is shown. For the adrenal source, the S-value ratio between Geant4 and MCNPX is shown above the bar for all target organs. The self-irradiation S-value for the adrenal source was not included in the plot due to substantial difference in order of magnitude comparing to the cross-irradiation S-values. Organ abbreviation: UB, urinary bladder; LLI, lower large intestine; ULI, upper large intestine; SI, small intestine; St, stomach.

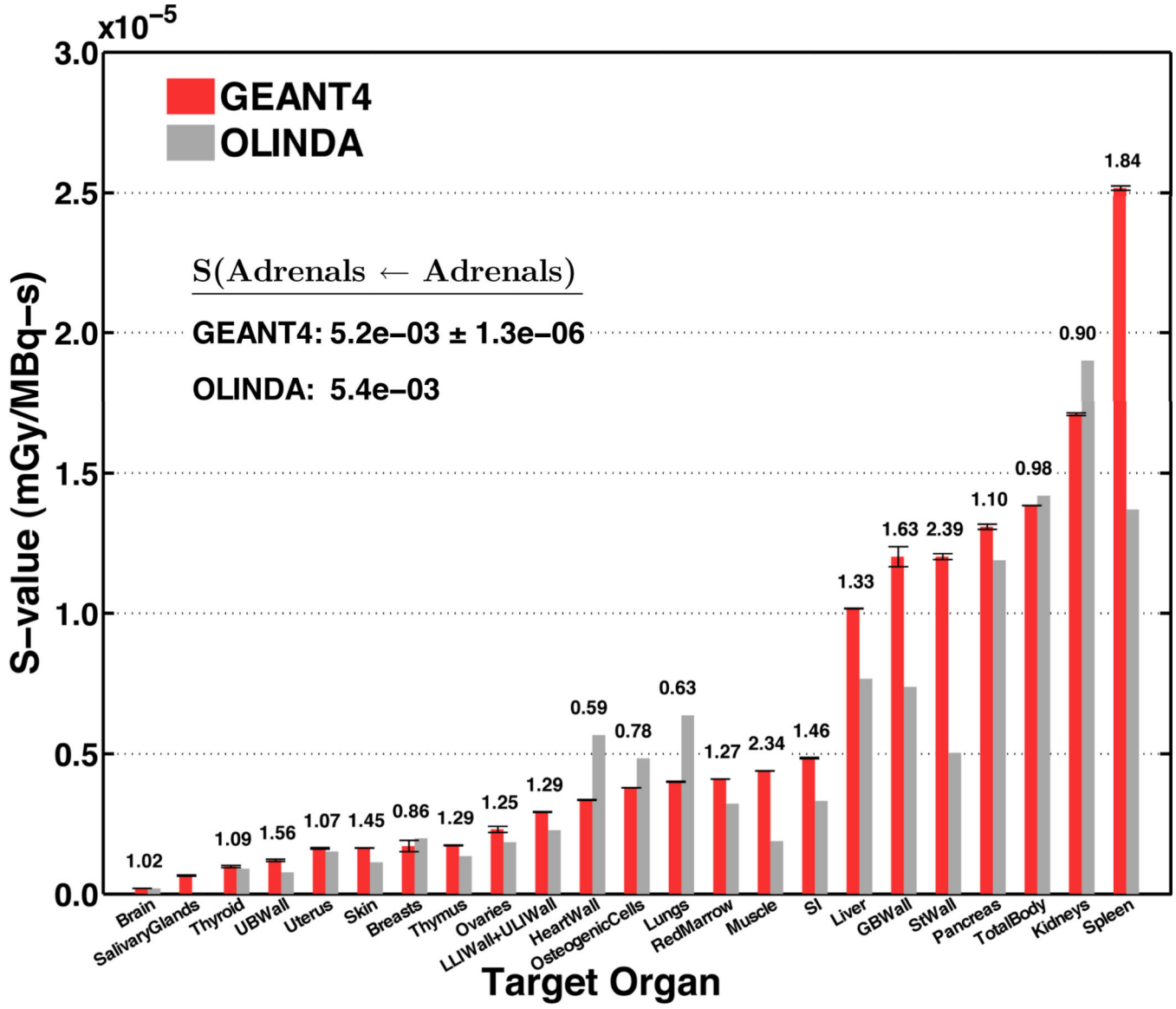

Figure 2.

The comparison of the I-131 S-value (mGy/MBq-s) ± standard deviation for the newborn model between the Geant4 method (left red bar) and OLINDA|EXM (right gray bar) is shown. For the adrenal source, the S-value ratio between Geant4 and OLINDA|EXM is shown above the bar for all target organs. The self-irradiation S-value for the adrenal source was not included in the plot due to substantial difference in order of magnitude comparing to the cross-irradiation S-values.

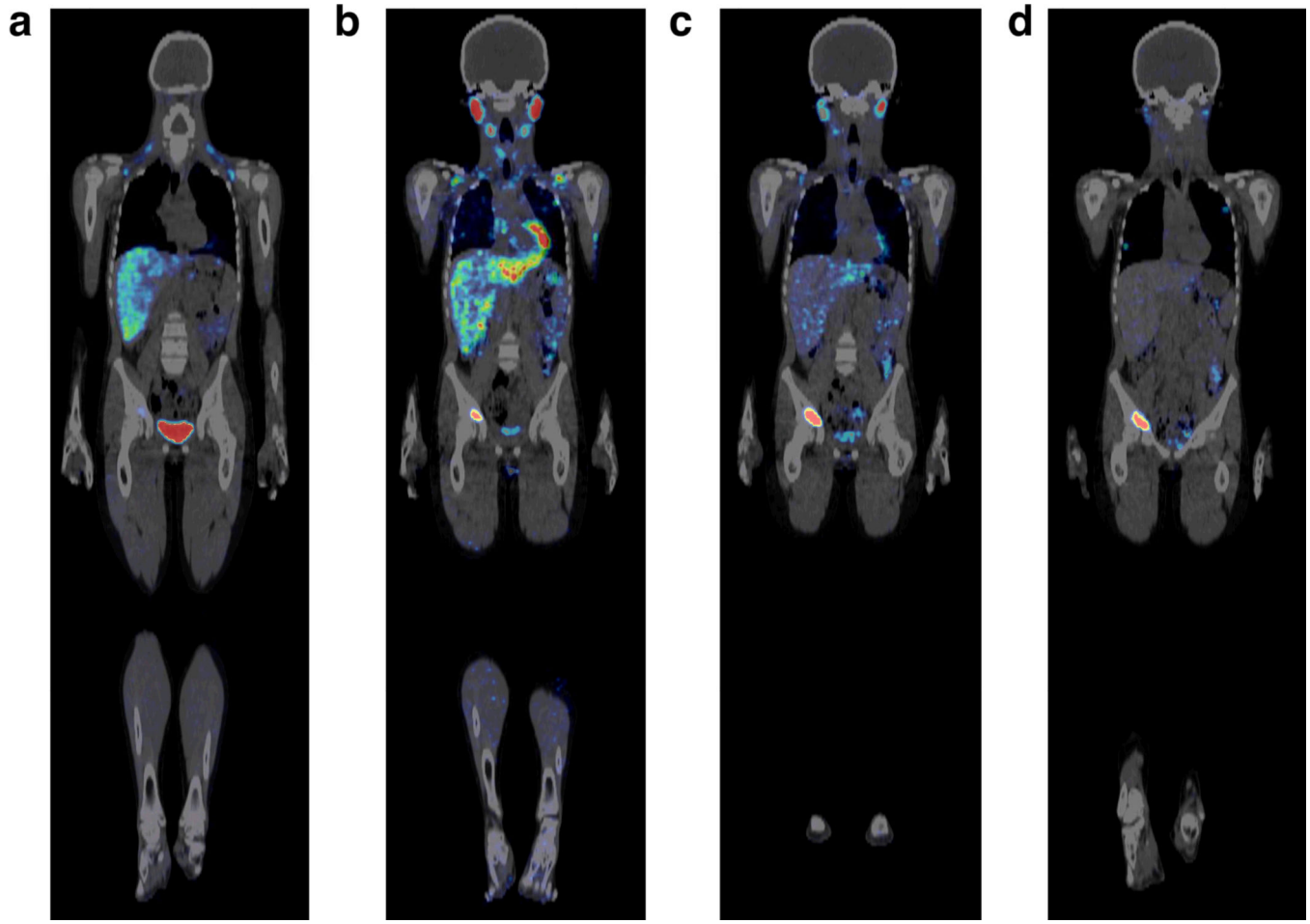

Figure 3.

The coronal view of the [^{124}I]mIBG PET/CT images for the patient in this study is shown for **a** 1.5 hr, **b** 19.5 hr, **c** 43.5 hr, and **d** 115 hr after injection of [^{124}I]mIBG.

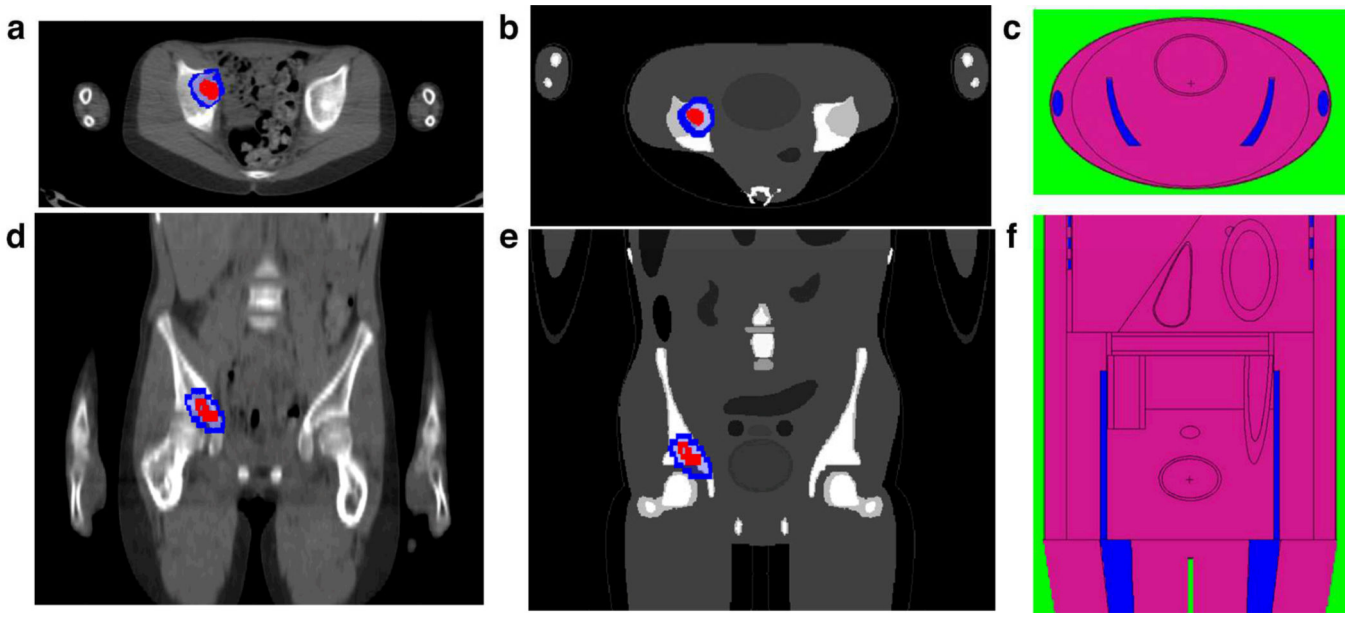

Figure 4.

The geometry assumed in the Geant4 and OLINDA dosimetry method is compared with the clinical CT images. The transverse view of **a** the clinical CT image, **b** the UF/NCI 10-year-old female phantom image, and c the stylized phantom used in OLINDA are compared. **d, e, and f** are the images of the clinical CT image, the UF/NCI female phantom, and the stylized phantom in the coronal view. The VOIs contoured for the [^{124}I]mIBG quantification (blue) and the metabolic tumor volume (red) of lesion #2 are illustrated on the clinical CT image and the UF/NCI phantom image.

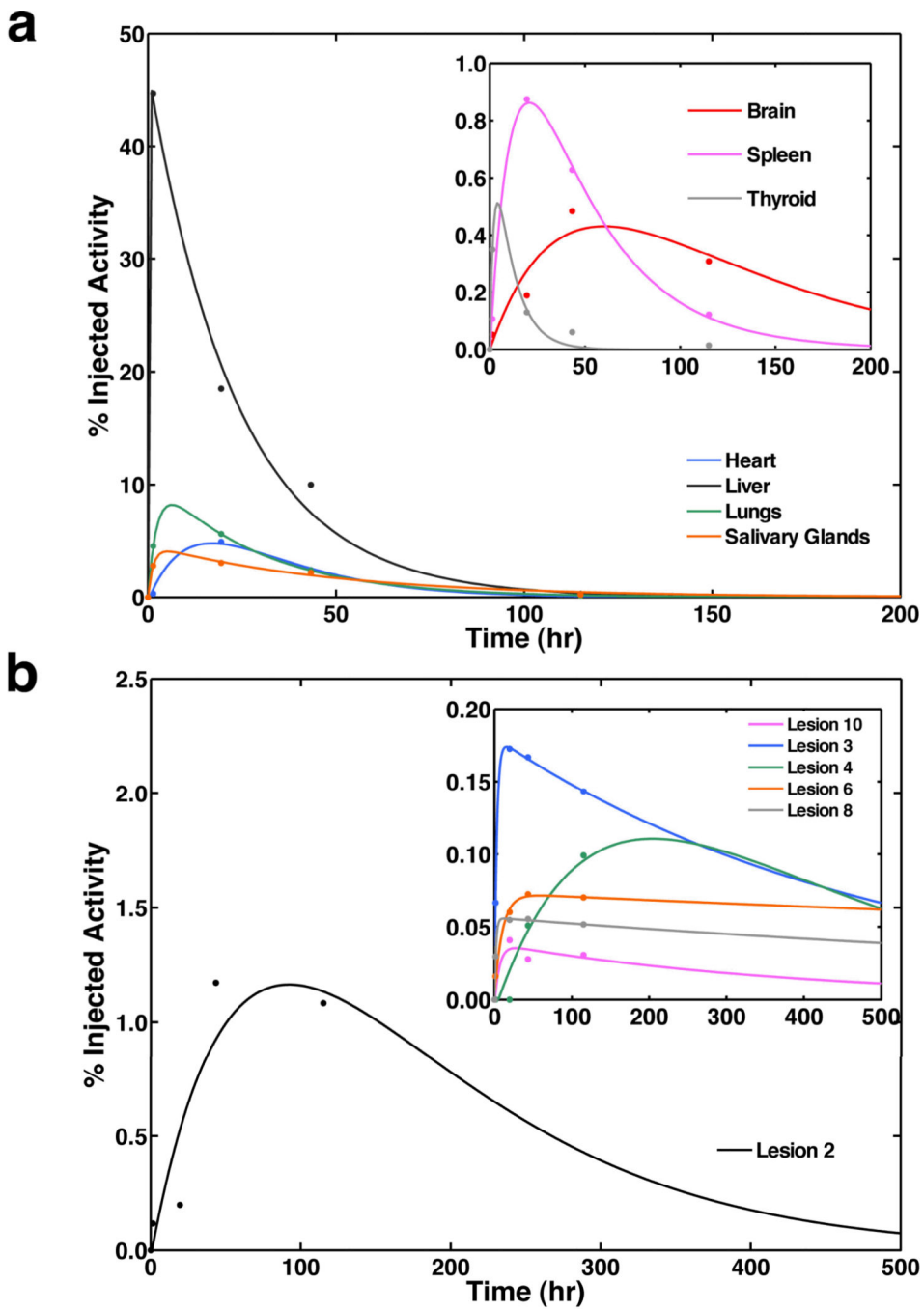

Figure 5.

The time activity curves (%IA as a function of time) quantified from the [^{124}I]mIBG PET images of the 10-year-old girl are shown for **a** source organs including heart, liver, lungs, salivary glands, brain, spleen, and thyroid and **b** six lesions. The solid dot is the original data, and the solid line is the bi-exponential fit of the original data.

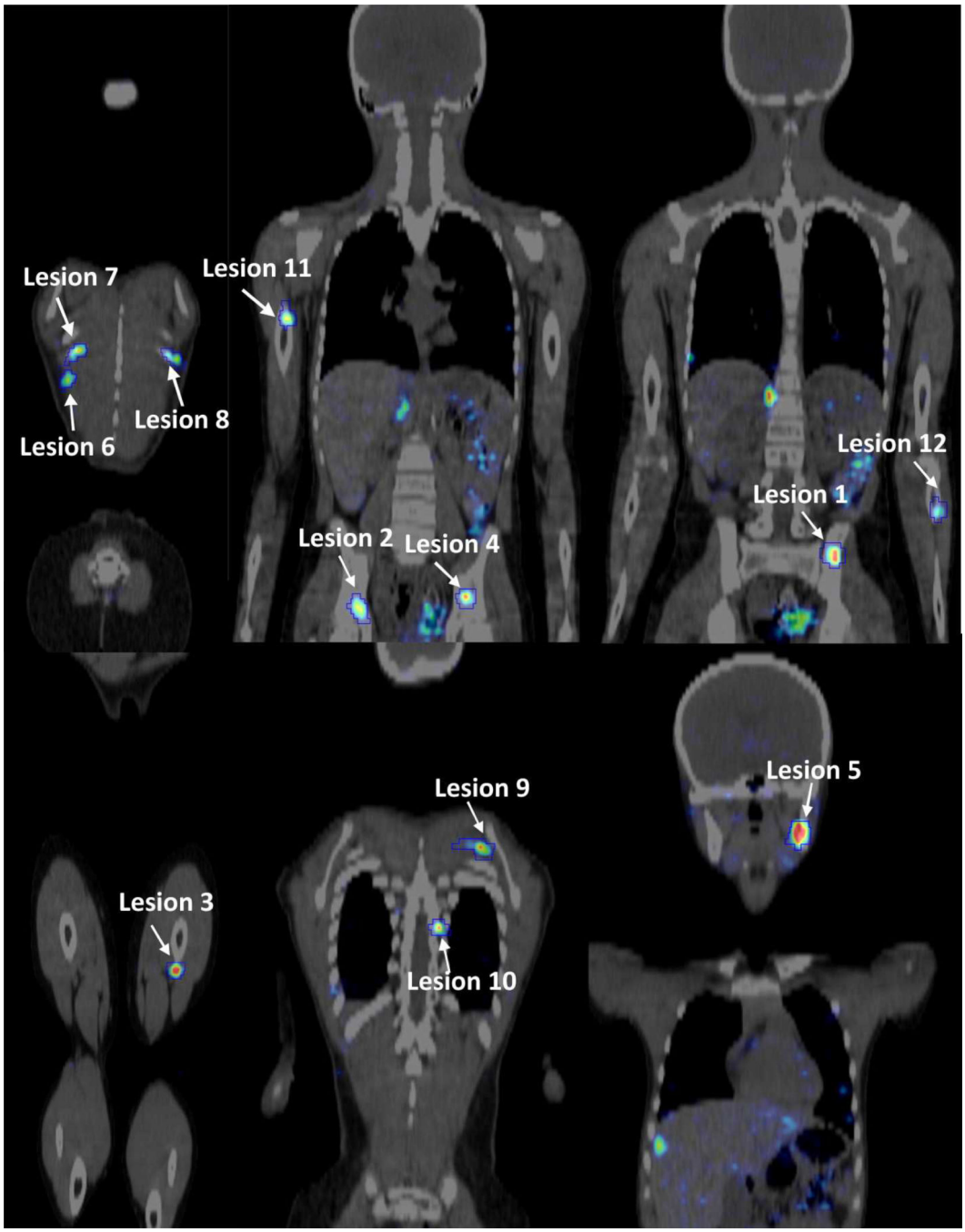

Figure 6.
The locations of the 12 lesions considered in this study are identified in the [^{124}I]mIBG PET/CT images of the clinical case at 115-hr after injection.

Table 1

The [^{131}I]mIBG residence time (MBq-hr/MBq) estimated in this study is compared to those in other murine and human studies.

Source Organ	[^{131}I]mIBG Residence Time (MBq-hr/MBq)		
	[^{124}I]mIBG PET/CT in animals (Lee *et al.*, 2010)	[^{131}I]mIBG in Human (Coleman *et al.*, 2009)	[^{124}I]mIBG PET/CT in Human (this study)
Salivary glands	n/a	1.10 ± 0.36	1.9
Thyroid	0.53 ± 0.17	0.45 ± 0.15	0.07
Lungs	3.27 ± 1.22	2.97 ± 0.95	2.6
Heart	0.88 ± 0.09	0.80 ± 0.20	1.9
Liver	5.03 ± 1.38	5.37 ± 2.74	10.2
Spleen	n/a	0.82 ± 0.30	0.48
Brain	n/a	0.54 ± 0.16	0.47
Urinary bladder	1.20 ± 0.25	2.01 ± 0.14	1.07
Total body	30.33 ± 5.45	36.54 ± 65.18	47.1
Remainder body	18.86 ± 6.64	23.25 ± 20.39	25.0

Table 2

The metabolic tumor volume (cm^3), the [^{131}I]mIBG residence time quantified from the pretherapy [^{124}I]mIBG PET/CT images, the absorbed dose estimated by the dosimetry method in this study, % of the total absorbed dose from the cross-irradiation, and % of the total absorbed dose from the self-irradiation are listed for all lesions identified in the clinical case in this study.

Tumor #	Metabolic Tumor Volume (cm^3)	[^{131}I]mIBG Residence Time (MBq-hr/MBq)	Absorbed Dose (Gy)	% Self Dose	% Cross Dose
Lesion 1	0.87	0.461	946.27	99.80	0.20
Lesion 2	3.59	1.634	892.16	99.78	0.22
Lesion 3	0.37	0.317	1331.61	99.90	0.10
Lesion 4	0.19	0.199	1641.32	99.88	0.12
Lesion 5	0.57	0.312	886.88	99.08	0.92
Lesion 6	0.52	0.179	505.23	99.24	0.76
Lesion 7	0.36	0.116	522.29	99.23	0.77
Lesion 8	0.33	0.129	637.26	99.50	0.50
Lesion 9	1.36	0.219	253.94	91.17	8.83
Lesion 10	0.17	0.061	461.31	99.36	0.64
Lesion 11	0.50	0.099	312.26	99.31	0.69
Lesion 12	0.56	0.049	143.86	99.31	0.69

Table 3

The absorbed dose (Gy) estimated by the patient-specific dosimetry method using the Geant4 method and the pretherapy [^{124}I]mIBG PET/CT imaging is shown for the major target organs for the clinical case in this study.

Target organ	Absorbed Dose (Gy)
Brain	1.46
Osteogenic Cells	1.84
AM	2.25
Skin	2.72
Muscle	3.77
Colon Wall	3.84
SI	3.99
Breasts	4.06
Kidneys	4.50
Total Body	4.88
Thymus	4.93
Ovaries	4.94
Pancreas	4.96
Uterus	5.07
Stom Wall	5.14
Right Adrenal	5.91
UB Wall	6.01
GB Wall	7.63
Spleen	15.96
Lungs	21.16
Thyroid	22.56
Liver	34.27
Hrt Wall	36.49
Salivary Glands	98.02